E9-2014-8

V. L. Smirnov, S. B. Vorozhtsov, J. Vincent[1]

H^- SUPERCONDUCTING CYCLOTRON FOR **PET** ISOTOPE PRODUCTION

Submitted to «Письма в ЭЧАЯ»

[1] Ionetix Corporation, Lansing, MI 48911, USA

Смирнов В. Л., Ворожцов С. Б., Винцент Дж. E9-2014-8
Сверхпроводящий H^--циклотрон для производства изотопов для ПЭТ

Разработан физический проект компактного сверхпроводящего циклотрона, ускоряющего H^--ионы до энергии 14 МэВ и предназначенного для получения радиоизотопов ^{18}F и ^{13}N. Ускоритель отвечает основным требованиям, предъявляемым к медицинским машинам. В частности, компактные размеры циклотрона обеспечиваются за счет использования сверхпроводящего магнита. Расчеты показали, что предлагаемая установка способна производить пучки протонов с током свыше 500 мкА. Для повышения надежности системы и увеличения ее производительности применяется внешний источник H^--ионов. В работе выполнены выбор концепции циклотрона, разработка его структурных элементов, расчет электромагнитных полей и динамики пучка от ионного источника до системы вывода из установки.

Работа выполнена в Лаборатории ядерных проблем им. В. П. Джелепова ОИЯИ.

Препринт Объединенного института ядерных исследований. Дубна, 2014

Smirnov V. L., Vorozhtsov S. B., Vincent J. E9-2014-8
H^- Superconducting Cyclotron for PET Isotope Production

The scientific design of a 14-MeV H^- compact superconducting cyclotron for producing of the ^{18}F and ^{13}N isotopes has been developed. Main requirements to the facility as a medical accelerator are met in the design. In particular, the main requirement for the cyclotron was the smallest possible size due to the superconducting magnet. The calculations show that the proposed cyclotron allows extracted beam intensity over 500 μA. To increase system reliability and production rates, an external H^- ion source is applied. The choice of the cyclotron concept, design of the structure elements, calculation of the electromagnetic fields and beam dynamics from the ion source to the extraction system were performed.

The investigation has been performed at the Dzhelepov Laboratory of Nuclear Problems, JINR.

Preprint of the Joint Institute for Nuclear Research. Dubna, 2014

1. INTRODUCTION

The U.S. Food and Drug Administration on October 25, 2013 approved Vizamyl (flutemetamol ^{18}F injection), a radioactive diagnostic drug for use with positron emission tomography (PET) imaging of the brain in adults being evaluated for Alzheimer's disease (AD) and dementia [1]. This recent event suggests a much larger supply of the ^{18}F-Fluoride radioisotope well beyond the current production capacity will be needed soon.

The goal of this project is to develop a 14-MeV H^- compact superconducting cyclotron with a cryogen-free magnet small enough to place multiple new machines in place of an existing conventional machine into an existing vault. The machine will be designed to extract 500 μA of current exceeding the capability of most existing conventional machines for the production of ^{18}F-Fluoride radioisotopes. This provides for existing facilities to economically at least double production capacity while simultaneously increasing system reliability through redundancy. Other PET isotopes may also be produced with this machine such as ^{13}N ammonia that provides for superior blood flow imaging in cardiology applications.

The H^- source for this machine must be efficient and reliable. To increase system reliability and production rates, an external ion source will be applied. This requires the machine to be designed with a sufficient axial bore through the steel to allow for installation of a spiral inflector and the associated simplest possible Low Energy Beam Transport (LEBT) system. The ion source can be biased to whatever voltage needed to get the initial energy but this must be balanced against the needed spiral inflector voltage. The spiral inflector becomes a problem the higher the bias due to flashover and plating of the insulators. We must balance the required voltage against the need for an extremely trouble-free design. We may even be clever enough to make use of the cyclotron fringe field to enhance the source.

The RF system for this machine consists of two 90° dees operated at 180° RF phase connected to tuning stems emanating from one side of the magnet. The other side of the magnet is reserved for the extraction system. This arrangement, although more complex than a simple single-dee structure, should provide about 40% more acceleration per turn assuming the same dee voltage at about 1/2 the drive power as compared with a single-dee structure.

Table 1. Main cyclotron parameters

Parameter	Value
Type	Compact, isochronous
Ion	H^-
Injection type	Axial, spiral inflector
Injection energy	25 keV
Central magnetic field	3.5 T
RF frequency	53.36 MHz
Dee voltage	40 kV
Extraction energy	14 MeV
Extraction type	Stripping foil
Beam intensity	500 μA
Final radius	148 mm
Cyclotron diameter	840 mm
Cyclotron height (with injection line)	1520 mm

Computer simulations of the cyclotron (magnet, beam dynamics, RF system) have been conducted and the main parameters of the cyclotron are given in Table 1. A general view of the machine is shown in Fig. 1.

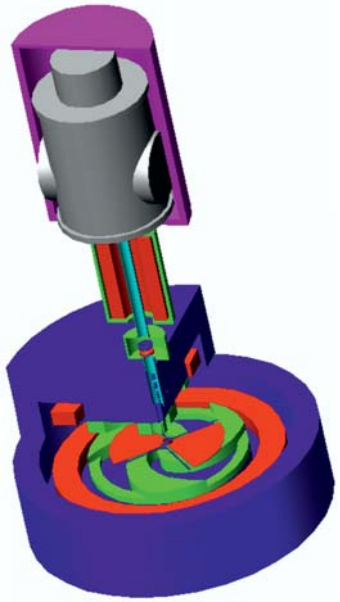

Fig. 1. Computer model of the cyclotron

2. MAGNET

The magnet will consist of room temperature yoke and pole steel with either one or two cryostats to be determined during the engineering design containing the superconducting coils. The cryostat(s) will be cryogen-free featuring conduction cooled coils. This design eliminates the issues associated with cryogenic fluid supplies, safety, and cost and provides for the most space available to other critical subsystems such as the ion source, RF system, and extraction systems.

The superconducting coil is surrounded by ~ 2 cm of space for the thermodynamics requirements and then likely ~ 0.63 cm of stainless steel to allow for each coil to be housed in its own cryogen-free cryomodule. The thermodynamics requires at a minimum 2 cm of internal space between the coil and the warm surfaces and 1 cm of space for the vessel walls and spacing. Thus, we allocate 3 cm of clearance all around the coil in the design. The design allows for a separate coil cryostat for the upper and lower coils with 3 radial and 3 vertical links for each. Coil forces can be coped with, but it is preferred that axial coil forces remain in the same direction during energizing and steady state operation.

Table 2. Main magnet parameters

Parameter	Value
Outward diameter	840 mm
Height	450 mm
Pole radius	220 mm
Vertical gap between sectors	36 mm
Number of sectors	3
Sector angle	$60-43^\circ$
Spiral angle	55°
Coil current density	130 A/mm^2
Weight	1.55 ton

The main magnet parameters are given in Table 2. To allow for H^- lifetime issues due to magnetic and vacuum stripping, a conservative value of 3.5 T for the central magnetic field was chosen. This value introduces some peculiarities in the design of the main magnet. In particular, at the above-mentioned level of the field it is rather problematic to obtain sufficient magnetic field flutter with radial-sector shims since the contribution of the shims is limited by the saturation of the shim material. The way out is application of spiral-sector shims which number is chosen to be 3 for obtaining maximal flutter value.

At this point in the design, the main requirement for the cyclotron was the smallest possible size of the magnet. This is why the spiral angle of the sector

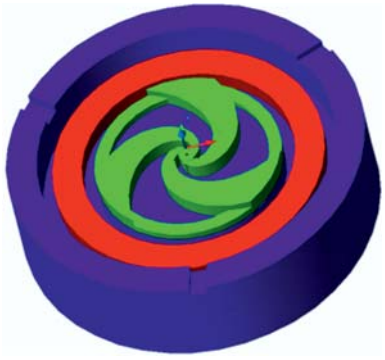

Fig. 2. Computer model of the cyclotron magnet

shims was selected rather large, namely 55°, and the isochronous field shaping was performed by varying the angular width of the spiral sectors and valley shims near the final radius, while the axial air gaps between the spirals and the poles were kept constant (see Fig. 2). As was mentioned above, the superconducting coil requires 3-cm space around for the thermoisolation layer. The dimensions of the magnet yoke were taken as small as possible given its contribution to the magnetic field level in the air gap between the magnet poles. At the design stage, an analysis and suppression of the magnet fringe field were not dealt with.

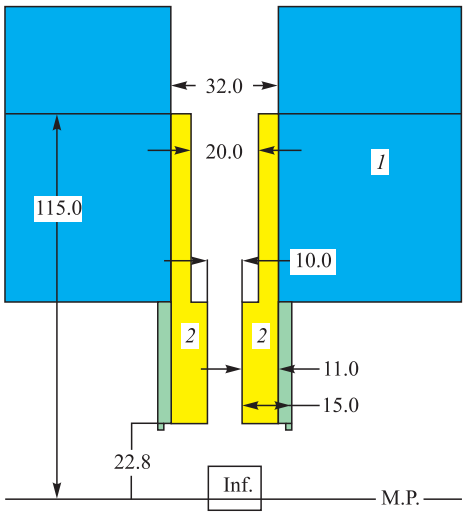

Fig. 3. Central plug cross section: *1* — pole, *2* — movable part

As was mentioned above, the accelerator design foresees axial beam injection. This is why the magnetic field shaping in the central region of the cyclotron is an important task to fulfill. A spiral inflector was used for the beam transportation from the axial injection line to the cyclotron midplane. An axial opening in the magnet yoke is used for installation of the spiral inflector in the central region. The compensation of the field perturbation due to this opening is not a trivial task since the size of the spiral inflector is comparable with the dimension of the central magnetic plug (Fig. 3) and even with the size of the whole acceleration zone. The opening with a radius of 16 mm for accommodation of the inflector produces a negative impact on the radial distribution of the mean magnetic field leading to the field dip in the central region. In the central region where the magnetic field rapidly increases with radius and there is no magnetic field flutter, stability of the axial particle motion is questionable. The solution of the problem would be separation of the plug into fixed and moveable parts (Fig. 3, *2*). The latter can be taken from the central region together with the inflector as a single unit.

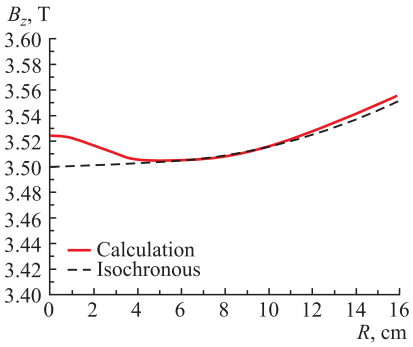

Fig. 4. Mean magnetic field

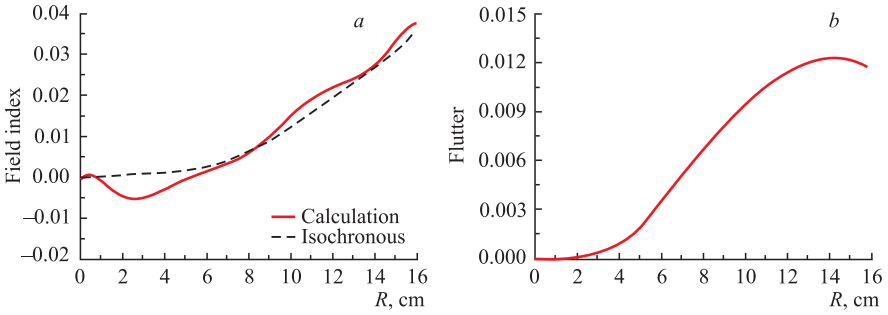

Fig. 5. Field index (a) and flutter (b) vs. the radius

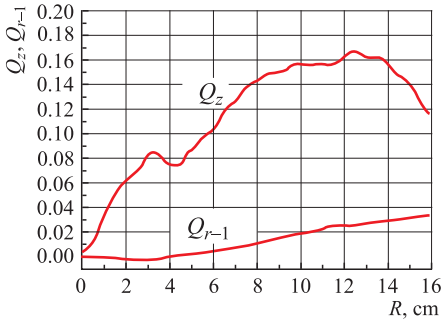

Fig. 6. Betatron tunes

The results of the field shaping using the magnetic field software OPERA3D [2] are given in Figs. 4–6.

3. INJECTION LINE

The well-known TRIUMF Type DC Volume-Cusp ion source [3] can be considered as an injector of H^- ions. The source has an output current over 15 mA with a relatively small overall size.

At the initial design stage, several options of the injection line structure were considered. Some existing publications on the problem were thoroughly studied [4–6]. The main criteria in the accelerator project development were the minimal size, the weight of the facility, and the simplest design. The axial injection line was carefully investigated from this point of view. As a result, a solenoid was chosen as the only focusing element. This solution is similar to the Kolkata K500 cyclotron, which is the operational machine having in the injection line only one solenoid near the magnet yoke [7]. The idea was to effectively use a large fringe field of the main magnet for particle focusing in view of the fact that the magnet fringe field amounts to several kGs at a distance of several hundred mm from the center of the magnet.

The question of including an RF buncher in the injection line required a special investigation. For the 300-mm-long solenoid (40-mm aperture for the beam) and a buncher 100–120 mm long, the ion source can only be installed at a distance of $\sim$ 750 mm from the magnet midplane. Then the main magnetic field at the ion source location would be $\sim$ 1 kGs. This fact implies a necessity of shielding the source from the main magnetic field using iron plates around the source. The 3D calculation showed that 20-mm-thick shielding was enough to suppress the main magnetic field down to an acceptable value in the ion source area (Fig. 7). The shielding weighs about 150 kg (Fig. 8).

At the initial stage of the injection line structure design, including definition of its parameters, the Trace2D/3D matrix code was used [8]. In the Trace codes, the Z axis distribution of the combined solenoid and main magnet field, estimated by the OPERA3D program [2], was approximated by a sum of sub-solenoid fields.

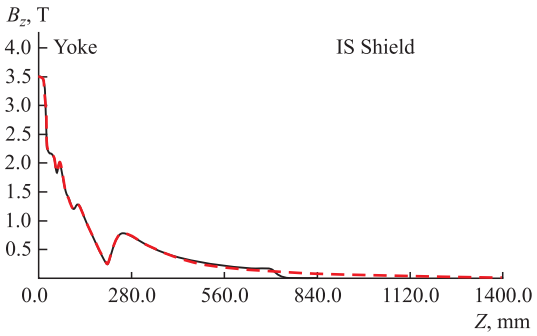

Fig. 7. Magnetic field shielding effect. The dashed line is the main cyclotron field, and the solid line is the field after shielding

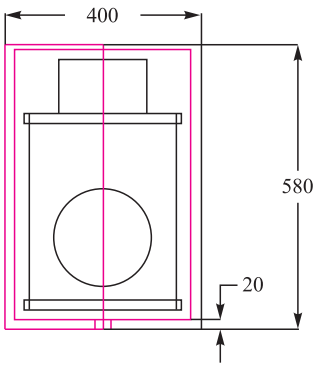

Fig. 8. Ion source shielding

The main magnetic field was taken into account along the Z axis up to the entrance to the shielding wall around the ion source. To confirm the results obtained with the Trace codes, comparable simulation by the SNOP multiparticle 3D code [9] was performed at low beam intensity for eliminating space charge effects from the benchmarking. The needed parameter adjustment to get almost coincident beam envelopes with the SNOP and the Trace3D is only $\sim 2\%$ of the original settings with the Trace2D giving the same result as the Trace3D in this case.

The solenoid field was chosen such as to match the beam size to the 3-mm inflector aperture at its entrance. Additional options without the solenoid and with complete main field shielding outside the magnet yoke were investigated. Calculations showed that the main magnetic field was very important for the beam focusing in the injection line. The solenoid field $\sim$ 2 kGs is optimal, ensuring the converging beam with a $\sim$ 2-mm spot size at the inflector entrance.

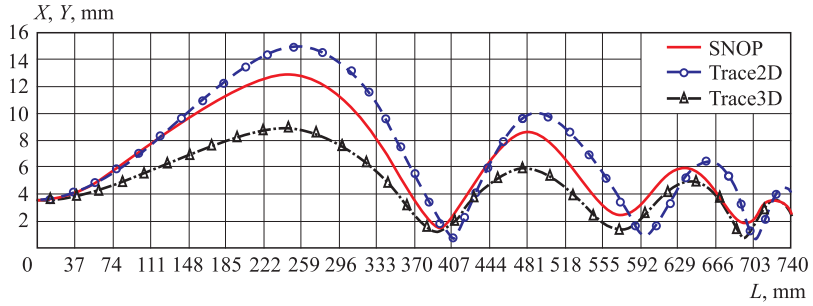

Fig. 9. SNOP/Trace2D/Trace3D results for the 15-mA beam from the ion source

The final selection of the injection line parameters was performed using SNOP code calculations with OPERA3D-calculated 3D distributions of the fields. The initial beam has 30,000 test particles with a Gaussian distribution within its measured transverse emittances $110\,\pi \cdot \mathrm{mm} \cdot \mathrm{mrad}$ [3]. The Particle-in-Cell (PIC) method was used for the beam self-field calculations. The parameters in the PIC method (the meshing granularity and the distance from the beam to the mesh boundary) were chosen using the calibration simulation of the injection line by the direct Particle-to-Particle (PP) method. The calculation took about 36 hours of computer time compared to the PIC method that took only 10 min to solve the same problem. The results of calculating the beam envelopes for the 15-mA beam intensity extracted from the ion source are shown in Fig. 9.

3.1. Sine-Wave Buncher. The experience with the buncher on the MSU K500 cyclotron [10] is that a simple first-harmonic buncher increases the transmission by about a factor of 3 and the tuning is relatively insensitive. Adding a second harmonic increases the transmission to about a factor of 5, but causes very high sensitivity to parameter variation. The buncher is placed axially immediately at the entrance to the yoke.

To decide on the necessity for including a buncher in the injection line, calculations were conducted on the beam dynamics from the ion source to the final radius in the cyclotron. The beam current at the final radius was estimated for various beam intensity from the ion source.

A 3D computer model of the buncher was constructed for the calculation of the buncher field (see Fig. 10) In the figure, truncated cones with a 5-mm gap are placed inside the ground case. The grids with a wire thickness of 50 μm and spacing 3 mm are used for shaping the uniform electrical field in the transverse direction.

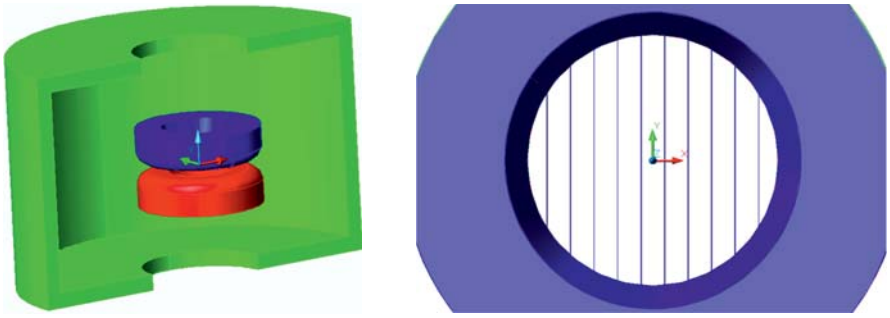

Fig. 10. 3D model of the buncher

The buncher transparency is $\sim 98\%$, and the aperture for the beam is 32 mm. The spatial distribution of the electrical field was calculated by the OPERA3D program [2]. The calculated field nonuniformity in the central plane of the air gap is less than 5%.

The schematic view of the whole facility with the axial injection line is shown in Fig. 11. It is seen that the size of the injection line is comparable with the size of the cyclotron itself. In the calculations it was assumed that the time variation of the buncher voltage had a sine-wave shape.

The longitudinal particle distribution in the median plane was analyzed to find the optimal buncher voltage. The inflector was excluded from the consideration at that stage. The goal of the optimization was to obtain the longitudinal beam focus in the midplane. The required buncher voltage was estimated to be 750 V. The buncher efficiency, i. e., the ratio of the particles with RF phases in the $\pm 20^\circ$ range to the total number of the particles in the injected DC beam in the $\pm 180^\circ$ range, was $\sim 42\%$ at the inflector entrance. In those calculations the beam space charge effects were excluded from the consideration. By definition, the buncher efficiency is 9% with the buncher switched off. The bunching efficiency decreases as the injected beam intensity and reaches $\sim 9\%$ at the beam current 15 mA. The effect can be explained by the Coulomb repulsion prevailing in the intense beam over the longitudinal focusing by the buncher. As a consequence, for a large enough injected beam current (8–9 mA) the buncher even decreases

the accelerated particle intensity compared to the case without the buncher. As an effect of using the buncher, the bunching gain factor, i. e., the ratio of the extracted beam intensities with and without the buncher, varies in the 2.9–0.64 range as a function of the injected beam current.

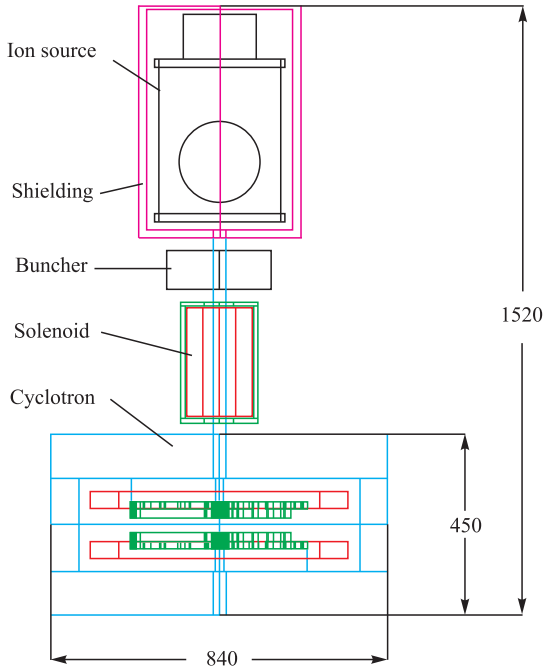

Fig. 11. Schematic view of the facility

One of the methods to increase the bunching efficiency is shifting the buncher closer to the magnet yoke. This leads to a weaker beam space charge effect due to a decrease in its action time. Obviously, a larger buncher voltage is needed in this case for providing the longitudinal beam focus in the midplane. In connection with the above-said, the structure with the solenoid first and the buncher downstream of the solenoid was investigated. The new buncher position is $Z = 305$ mm instead of previous 635 mm. In this layout Trace2D calculations show that the transverse dimension of the beam at the inflector entrance becomes even smaller than in the previous layout (Fig. 12). Similar to the previous layout, the bunching efficiency decreases with the injected beam intensity (Fig. 13), but at the inflector entrance the number of particles in the $\pm 20^\circ$ RF range becomes larger. Apparently, the required buncher voltage should be increased from 750 to 1670 V to get the longitudinal beam focus in the midplane.

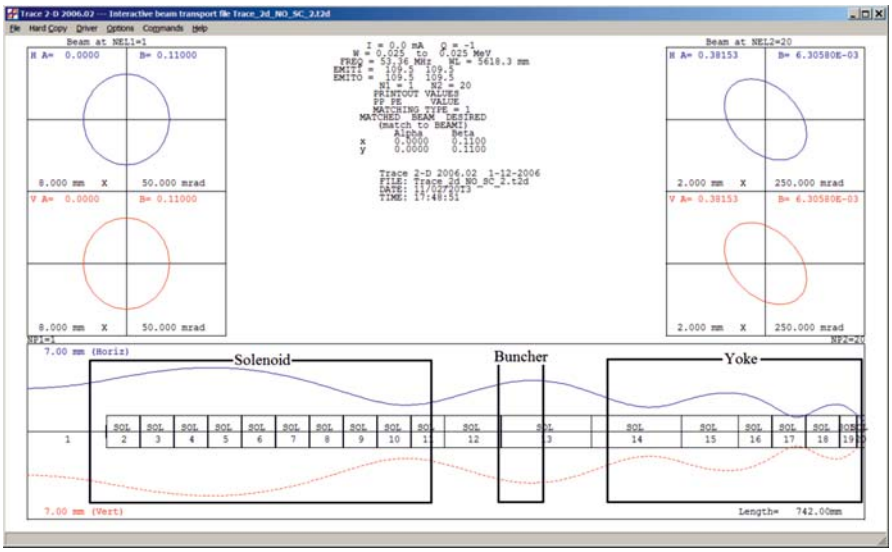

Fig. 12. Trace2D calculation. Injection line: ion source, solenoid, and buncher

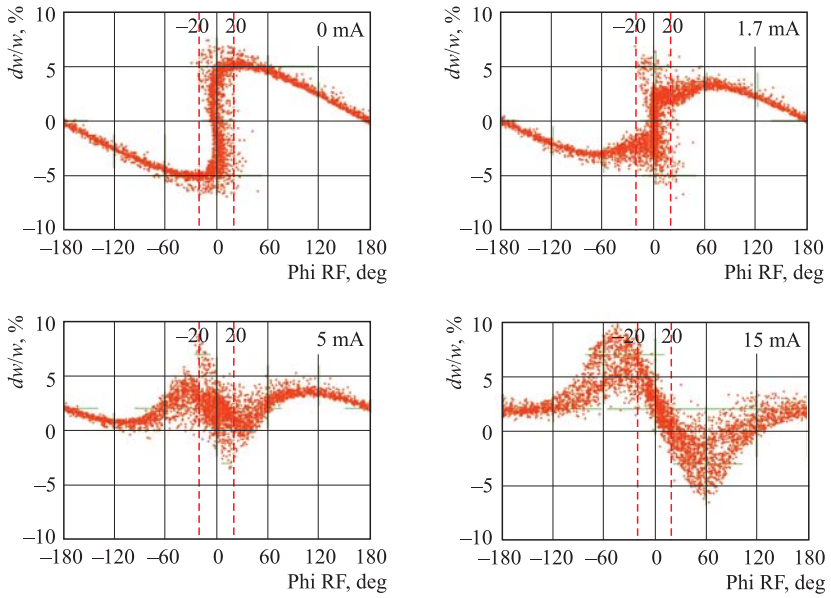

Fig. 13. Longitudinal beam distribution at the inflector entrace

Dependence of the accelerated beam intensity and bunching gain factor on the injected beam current is given in Tables 3 and 4. It can be seen that for all injection currents the accelerated beam intensity with the buncher is higher than without buncher when the buncher is closer to the magnet yoke. The effect can be explained by a smaller transverse beam emittance at the inflector entrance.

Table 3. Overall transmission (%)/Extracted current (μA)

Ion source current, mA	Axial buncher location 635 mm		Axial buncher location 305 mm		
	Without buncher	With buncher	Without buncher	With buncher	Gridless buncher
0.0	5.3	15.4	5.5	17.3	15.7
1.7	4.3/70	9.9/165	4.7/79	13.4/228	14.4/240
5.0	3.8/190	4.7/235	4.3/216	9.2/460	9.2/460
7.5	3.3/250	3.4/251	4.0/300	7.0/525	6.9/516
10.0	3.3/330	2.5/250	3.6/363	5.5/550	5.7/570
12.5	2.6/330	2.2/275	3.1/384	3.9/488	4.1/512
15.0	2.5/375	1.6/240	3.1/458	3.2/480	3.5/525

Table 4. Bunching gain factor

Ion source current, mA	Axial buncher location 635 mm	Axial buncher location 305 mm	
		Buncher with grid	Gridless buncher
0.0	2.90	3.15	2.85
1.7	2.30	2.85	3.06
5.0	1.24	2.14	2.14
7.5	1.03	1.75	1.73
10.0	0.76	1.53	1.58
12.5	0.85	1.26	1.32
15.0	0.64	1.03	1.13

The difference of the results for two structures without the buncher can be explained by different positions of the solenoid. The results also show that one of the major factors limiting the cyclotron output intensity is space charge effects in the LEBT. According to the calculation, the optimal injection beam intensity determined by these effects is 10 mA. Another limiting factor is loss of particles in the central region of the machine mostly due to mismatch between

the longitudinal beam emittance and the central region acceptance. Additionally, there is some axial loss as well, although at a lower scale. The importance of these effects for the final beam intensity will be shown below.

Next, a buncher without grid wires was investigated since these wires were always a source of failure. In this case a smaller aperture for the beam leads to similar results, eliminating maintenance issues. For the estimation of the gridless buncher, the LEBT layout with the buncher closer to the magnet yoke was considered. In addition to a gain in the transmission, this variant has a smaller beam size at the buncher location, allowing a smaller buncher aperture for the beam: 20 mm instead of previous 32 mm.

Some concern can be expressed regarding an amount of current hitting the buncher electrodes. To cure it, an upstream grounded collimator ring can be added to intercept this beam along with increasing the buncher aperture. But in our case the buncher aperture for the beam was chosen such as to eliminate almost completely particle loss. The multiparticle simulations with beam space charge effects included show that for experimentally measured emittance of the beam emerging from the ion source there is practically no loss on the buncher electrodes. Before the beam simulation the 3D electrical field was estimated for the gridless buncher. In this case, as expected, the transverse field uniformity becomes worse and the field magnitude becomes smaller (Fig. 14).

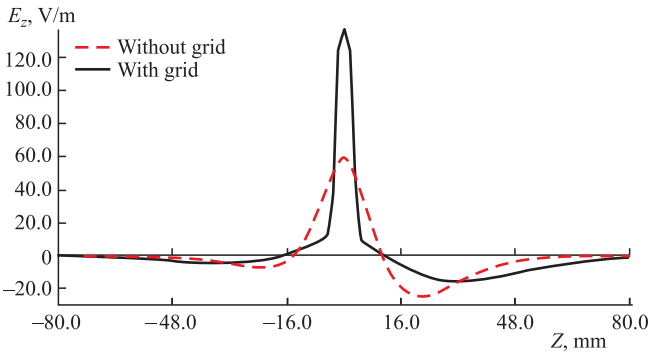

Fig. 14. E_z component vs. the Z coordinate

The multiparticle tracing confirms the above prediction: the gridless buncher practically does not affect the beam characteristics. A possible explanation can be that the integral of the absolute value of the axial electrical field component E_z along the Z axis remains practically the same in both cases. Figure 14 shows that for the chosen buncher electrode configuration the E_z field reverses the sign at a distance of ± 16 mm from the center of the buncher, i. e., the Z-width of the positive E_z range is ~ 32 mm. But for the given injection energy 25 keV and RF frequency 53.36 MHz the $\pm 180^\circ$ RF bunch length is ~ 41 mm,

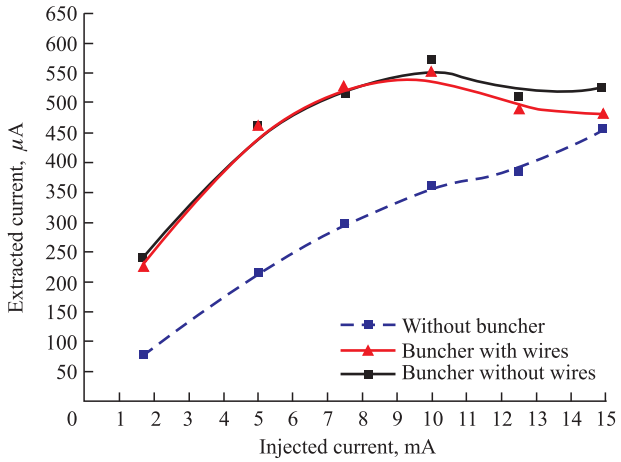

Fig. 15. Extracted beam current vs. the injected beam intensity

comparable with the 32-mm positive E_z Z-width. To see the importance of the negative E_z part of the field distribution, it was suppressed in the calculations. As a result, the extracted beam current reduced from 570 to 440 μA, which proves our explanation. Figure 15 shows the dependences of the extracted beam intensity on the injected beam current.

4. CENTRAL REGION

4.1. Inflector. A design of the accelerator's central region with a magnetic field of 3.5 T and external axial injection is not a trivial task. It is difficult to provide necessary conditions for avoiding large particle loss on the inflector case during the first turn of acceleration. A possible solution of the problem would be an increase in the dee voltage, but in our case this is not acceptable since the dee voltage is limited to 40 kV. So, the problem of increasing the central region efficiency is mainly reduced to minimization of the inflector size. A 3D computer model of the inflector is shown in Fig. 16.

When designing the inflector we optimized some of the main relations for its parts. For example, the inflector aspect ratio (electrode width over air gap size between electrodes) was chosen to be 1.67 instead of the commonly adopted value above 2, although in some publications the authors propose decreasing the aspect ratio down to 1.25 [11]. But in this case a serious problem of the field non-uniformity in the gap between the electrodes leads to a substantial complication of the inflector design. The gap was reduced to 3 mm, although common practice

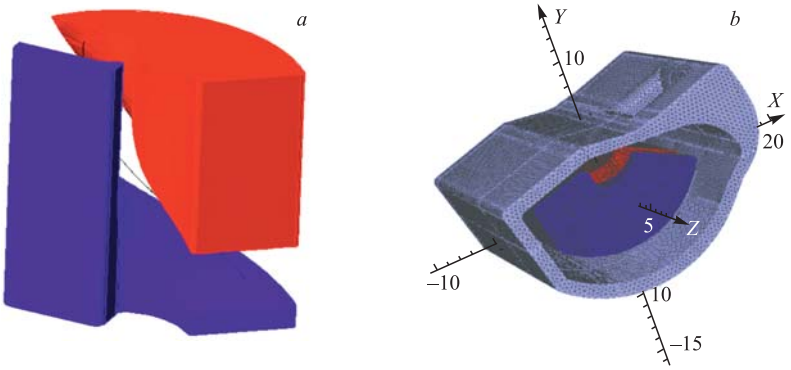

Fig. 16. Spiral inflector: the mechanical 3D model (a) and the OPERA3D model with the RF shield for calculation of the electrical field (b)

suggests an inflector with the gap no less than 4–6 mm. The inflector voltage is chosen to be ± 7 kV in view of the fringe field effect in the particle trajectories. The electrical radius is $R_e = 10$ mm and magnetic radius is $R_m = 6.5$ mm. Field and beam dynamics calculations show that this inflector allows transmitting a beam with sufficient effectiveness. It also does not introduce any beam quality distortion that could affect its further transmission through the central region. The calculations of the optimal electrode cutting at the end of the inflector for compensation of its fringe field have not been performed. The reference particle injected in the inflector experiences axial oscillations with amplitude less than 0.5 mm in the midplane downstream of the inflector.

4.2. Central Region Structure. As was mentioned above, the central magnetic field of the cyclotron is 3.5 T and the gyration frequency is 53.36 MHz. To get a maximal energy gain by particles in the 1st turn and most uniform distribution of the energy gain along the azimuth, it is reasonable to select a design with two 90° dees and to operate at the 2nd RF harmonic. But in this case the RF frequency would be ~ 107 MHz, which is too demanding from the point of view of maximal design simplicity and minimum energy consumption. In this connection we have to operate at the 1st RF harmonic, which makes the designing of the central region a rather laborious task. It requires providing not only a sufficient energy gain for particles to make initial turns in the cyclotron but also necessary focusing and centering of the beam. Figure 17 shows the structure of the central region in the cyclotron with the trajectory of the reference particle superimposed. The particle RF phase values at the location of the middle lines of the acceleration gaps are also indicated in the figure.

It is very important that particles cross the acceleration gaps at the 1st turn with a positive RF phase, i. e., at a decreasing dee voltage. This condition will

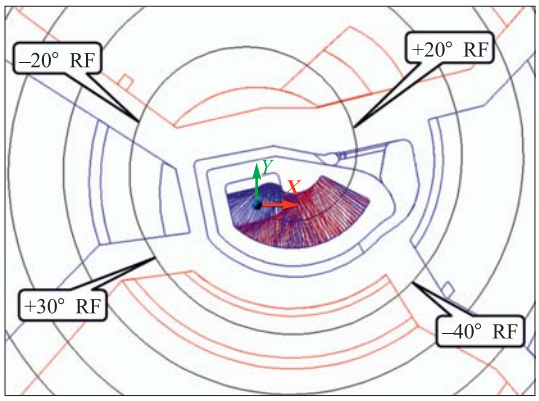

Fig. 17. Central region structure with the reference rarticle trajectory

provide axial focusing of the beam by the RF field. In the proposed design it was possible to cross only the 1st and the 3rd gaps with a positive RF phase. Naturally, the 2nd and the 4th gaps were crossed with a negative RF phase since the angular width of the dee is less than 180°. Nevertheless, the total axial focusing provided by the RF field and the magnetic bump in the central region is sufficient for stable axial motion there. The relative angular positions of the magnetic sectors and the central region electrodes were optimized to minimize radial oscillation amplitudes of accelerated particles.

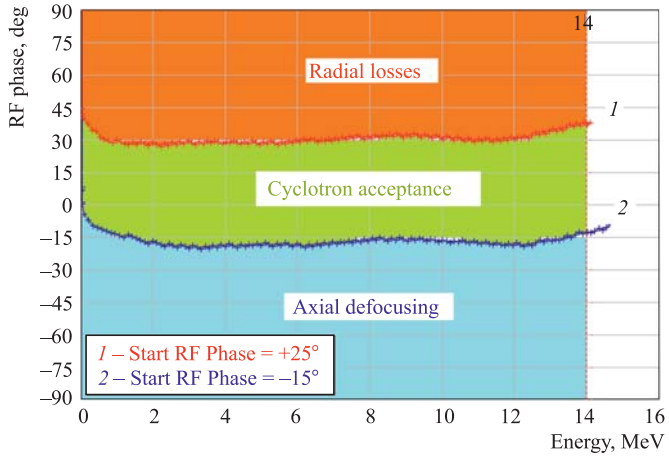

Fig. 18. RF phase excursion vs. the energy

Calculations show that the accelerator RF phase acceptance amounts to 40° (Fig. 18) with the zero RF phase corresponding to the particle acceleration at the maximal dee voltage. The acceptance was optimized by varying the relative positions of the inflector, dee tips, acceleration gaps and, which is most important, magnetic spiral sectors. The particles injected at an RF phase $\geqslant 25^\circ$ are lost in the initial turn due to insufficient energy gain at the dee gaps. When the injection is at a negative RF phase $\leqslant 15^\circ$, the axial ion motion becomes unstable. The quality of the mean magnetic field is such (in compliance with the isochronous condition) that the RF phase oscillation amplitudes are smaller than $\pm 5^\circ$.

5. MAGNETIC STRIPPING

Calculations were performed to check the electric dissociation of the ions. The results are given in Fig. 19 It can be seen that with a peak magnetic field of 3.5 T, the electromagnetic stripping in the cyclotron is negligible at a full

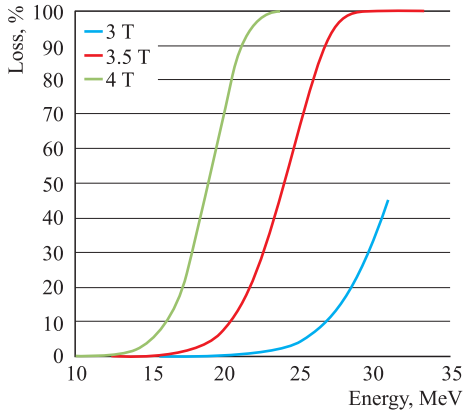

Fig. 19. H^- magnetic stripping, energy gain 40 keV/turn

energy of 14 MeV. For more accurate estimation of the effects, the azimuthal variation of the field, as well as its radial performance, should be taken into account in the calculation. The dissociation produced by the residual gas is another possible problem to be estimated depending on the average vacuum of the facility.

6. EXTRACTION SYSTEM

Particles make ~ 120 turns in the magnetic field before extraction with the dee voltage amplitude 40 kV. One-port stripping extraction is provided on this machine. The trajectory of the extracted particle is shown in Fig. 20. The stripping

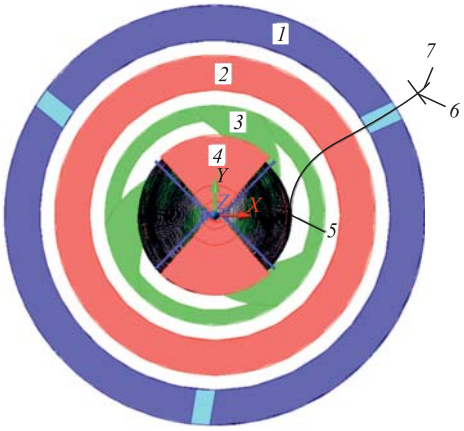

Fig. 20. Extraction from the cyclotron by stripping: *1* — yoke, *2* — coil, *3* — spiral shim, *4* — dee, *5* — stripping foil, *6* — production target assembly, *7* — extracted particle trajectory

foil $20\,\mathrm{mm} \times 20\,\mathrm{mm}$ in size was used in the simulation. The location of the foil was chosen at azimuth $0°$. The foil radius is 148 mm. The foil position allows extracting the beam through the yoke at the location free of the RF system. The production target assembly with a radius of 500 mm is located downstream of the so-called "Short Port" beamline [12] (see next section for description).

7. HIGH-ENERGY BEAM TRANSPORT

For the high-energy beam transport (HEBT) we intend to use the already developed successful system. For example, there is a work on this design (see Ref. [12]). It is a very short (150-mm-long) beamline known as the "Short Port" beamline that was developed for GE PETtrace$^{\mathrm{TM}}$ cyclotrons. It enables users to mount custom high performance targets on their machines. The "Short Port" beamline comes complete with a gate valve, four-jaw and water-cooled graphite collimator with beam current readbacks, a thermocouple

port, and, in the baseline version, a flange for mounting the Thermosyphon Target developed by Bruce Technologies for production of Fluorine-18. The device performed well, and met its functionality requirements. It may be used at our PET cyclotron.

Technical details of the target design are still to be decided, but some considerations are already available. The beam hits a water target with a window that can handle a $\sim$ 1-cm-diameter beam. So, the final beam quality is not much of an issue provided it falls within the target window. Many of the systems have multiple targets installed, so moving the stripping foil to shift the beam to other targets is likely the technique to be used. The GE PETtrace$^{\mathrm{TM}}$ machine target system [12] may yield some clues to design and operation requirements.

8. CYCLOTRON FUNCTIONALITY

The cyclotron functionality in terms of the beam transmission efficiency and the output beam quality is described in this section. The particles were traced from the ion source to the extraction port. The beam dynamics was analyzed using

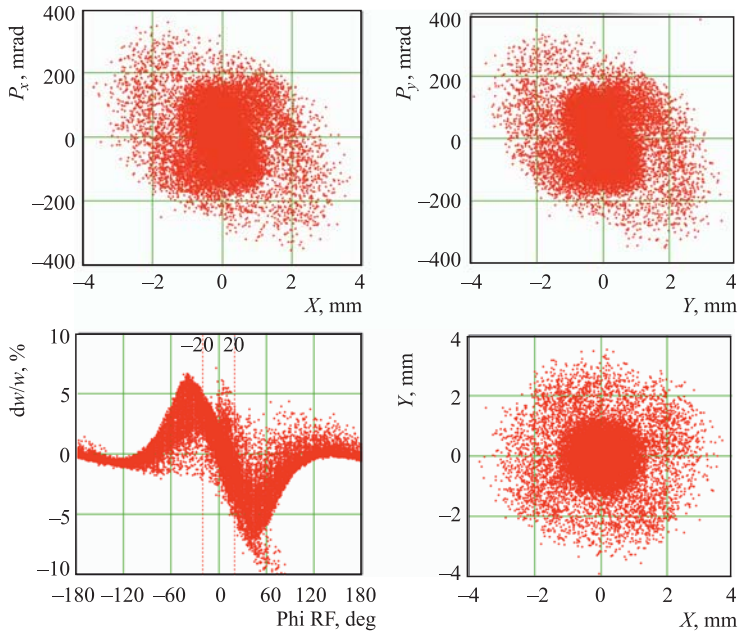

Fig. 21. Beam emittances at the inflector entrance for the gridless buncher and the optimal injected current of 10 mA

the SNOP program [9]. Calculations were performed using 3D electromagnetic fields obtained by OPERA3D and with the beam space charge effects taken into account.

The initial emittance for the simulation was generated at the ion source exit with the axial position 755 mm and represented by a Gaussian distribution. Transversal beam emittances equal $110\,\pi \cdot \mathrm{mm} \cdot \mathrm{mrad}$. The longitudinal beam length was taken to be 3 RF periods for accurate space charge calculations.

A gridless buncher located axially at a distance of 305 mm from the midplane was selected for simulations. The injected current was taken to be 10 mA. The beam emittances at the inflector entrance are shown in Fig. 21.

The beam loss distribution in the central region of the cyclotron is shown in Fig. 22. It is seen that the radial losses are concentrated near the structure elements like the pillar, post, RF shield and inflector, whereas the axial losses are scattered over the area being determined mostly by the dee axial aperture of 12 mm. Downstream of the region there are practically no particle losses, and, as a result, a beam of about 570-μA intensity is extracted by the stripping foil

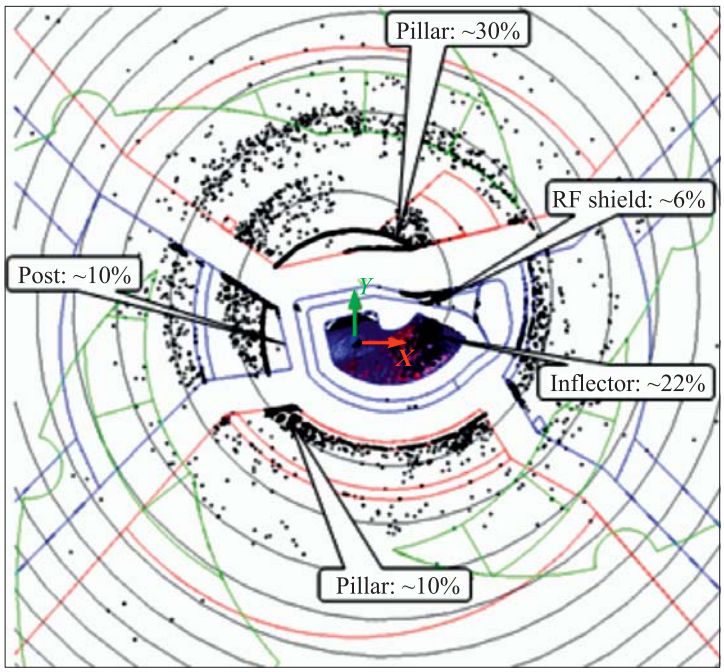

Fig. 22. Practicle loss distribution in the central region

with the characteristics given in Fig. 23. The effect of the multi-turn extraction is quite visible in the plot with longitudinal emittance of the beam.

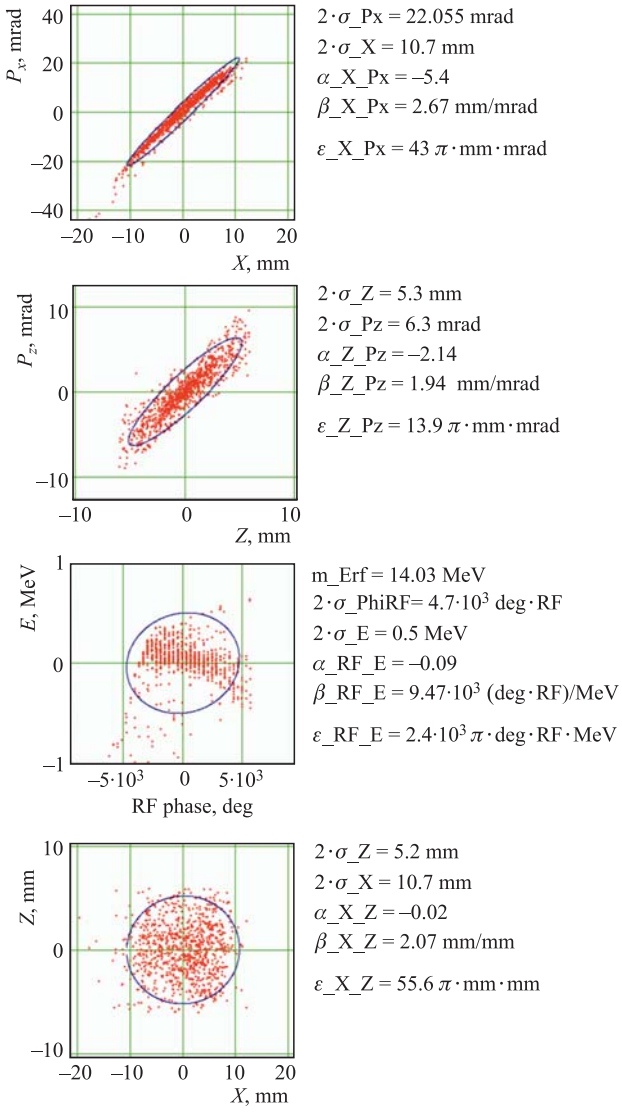

Fig. 23. Emittances of the extracted beam at the location of the production target assembly outside the cyclotron

9. SUMMARY

A preliminary design of a cyclotron for an H^- energy of 14 MeV is prepared. The choice of the cyclotron concept, design of the structure elements, calculation of the electromagnetic fields and beam dynamics including multiparticle simulations from the ion source to the extraction system were performed within a rather short period of time. The calculations show that the proposed cyclotron allows extracted beam intensity over 500 μA. It is worth noting that the above beam intensity is not final, and a more detailed analysis can improve quantitative and qualitative characteristics of the accelerated beam extracted from the cyclotron.

REFERENCES

1. http://www.fda.gov/newsevents/newsroom/pressannouncements/ucm372261.htm
2. Cobham CTS Ltd — Vector Fields Software. United Kingdom: Network House, Langford Locks, Kidlington, Oxfordshire, OX5 1LH.
3. *Kuo T. et al.* Development of a 15 mA DC H^- Multi-Cusp Source for Compact Cyclotrons // Proc. of the 14th Int. Conf. on Cyclotrons and Their Applications, Capetown, 1995.
4. *Kuo T. et al.* A Comparison of Two Injection Line Matching Sections for Compact Cyclotrons // IEEE. 1995. V. 3. P. 1858.
5. *An D. H. et al.* Beam Simulation of SQQ Injection System in KIRAMS-30 Cyclotron // Proc. of EPAC 2006, Edinburgh, Scotland.
6. *Dehnel M., Stewart T.* An Industrial Cyclotron Ion Source & Injection System // Proc. of the 17th Int. Conf. on Cyclotrons and Their Applications, Tokyo, Japan, 2004. P. 293–295.
7. *Dey M. K. et al.* Beam Injection System of the KOLKATA Superconducting Cyclotron // Proc. of the 18th Int. Conf. on Cyclotrons and Their Applications, 2007.
8. *Crandall K. R., Rusthoi D. P.* Documentation for TRACE: An Interactive Beam-Transport Code. Los Alamos National Laboratory Report LA-10235-MS (January 1985).
9. *Smirnov V. L., Vorozhtsov S. B.* SNOP — Beam Dynamics Analysis Code for Compact Cyclotrons // Proc. of the XXI Russian Accelerator Conference, RuPAC'2012, St. Petersburg, Russia, 2012.
10. *Stetson J. et al.* Intense Beam Operation of the NSCL/MSU Cyclotrons // Proc. of the 19th Conf. on Cyclotrons and Their Applications, Lanzhou, China, 2010.
11. *Garonna A.* Cyclotron Designs for Ion Beam Therapy with Cyclinacs // PhD Thesis, Ecole Polytechnique Federale de Lausanne, 2011.
12. *Theroux J. E. et al.* A "Short Port" Beamline for Mounting Custom Targets to a GE PETtrace^{TM} Cyclotron // Proc. of the 18th Int. Conf. on Cyclotrons and Their Applications, 2007.

Received on February 7, 2014.

Редактор *Е. И. Кравченко*

Подписано в печать 28.03.2014.
Формат 60 × 90/16. Бумага офсетная. Печать офсетная.
Усл. печ. л. 1,56. Уч.-изд. л. 2,15. Тираж 215 экз. Заказ № 58231.

Издательский отдел Объединенного института ядерных исследований
141980, г. Дубна, Московская обл., ул. Жолио-Кюри, 6.
E-mail: publish@jinr.ru
www.jinr.ru/publish/